Cell Reports

Article

# A spatial map of antennal-expressed ionotropic receptors in the malaria mosquito

## Graphical abstract

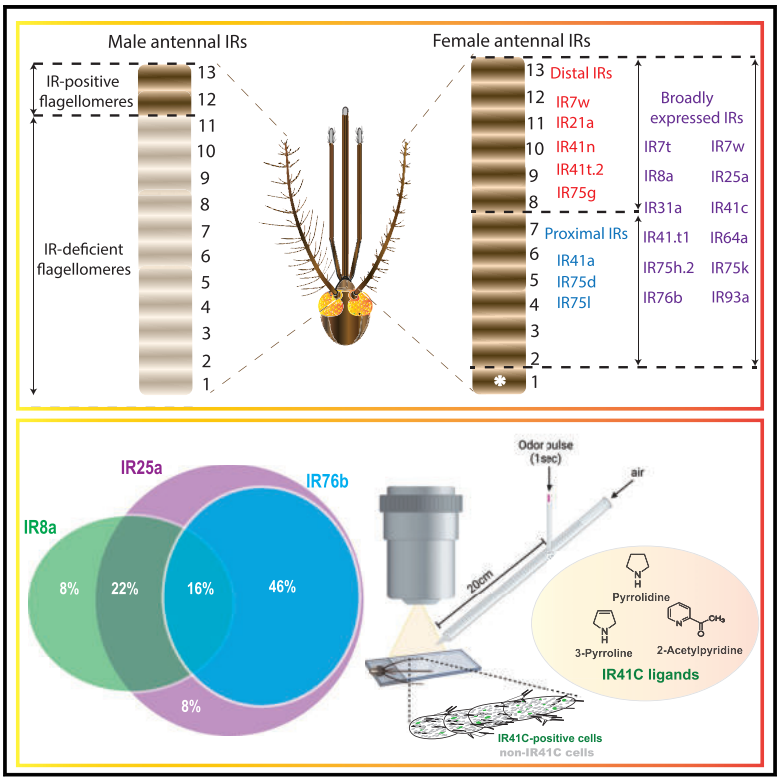


## Highlights

- Some antennal-expressed IRs are organized into proximal and distal domains
- IR coreceptor co-expression patterns offer functional insights into odor detection
- IR neuron populations are not changed after blood meal or in aged adults
- IR41c-expressing neurons are activated and inhibited by select amine compounds


## Authors

Joshua I. Raji, Joanna K. Konopka, Christopher J. Potter

## Correspondence

cpotter@jhmi.edu



## In brief

Raji et al. present the spatial organizational pattern of ionotropic receptor (IR) expression in the mosquito antenna. The IR map suggests general odor properties for IR neurons. A knockin of an odor-tuning IR supports the prediction and shows excitatory and inhibitory responses to odors.


Raji et al., 2023, Cell Reports *42*, 112101
February 28, 2023 
https://doi.org/10.1016/j.celrep.2023.112101

CellPress

Cell Reports

CellPress
OPEN ACCESS

Article

# A spatial map of antennal-expressed ionotropic receptors in the malaria mosquito

Joshua I. Raji,[1] Joanna K. Konopka,[1] and Christopher J. Potter[1,2,*]
[1]The Solomon H. Snyder Department of Neuroscience, Johns Hopkins University School of Medicine, Baltimore, MD 21205, USA
[2]Lead contact
*Correspondence: cpotter@jhmi.edu
https://doi.org/10.1016/j.celrep.2023.112101

## SUMMARY

The mosquito's antenna represents its main olfactory appendage for detecting volatile chemical cues from the environment. Whole-mount fluorescence *in situ* hybridization of ionotropic receptors (IRs) expressed in the antennae reveals that the antenna might be divisible into proximal and distal functional domains. The number of IR-positive cells appear stereotyped within each antennal segment (flagellomere). Highly expressed odor-tuning IRs exhibit distinct co-localization patterns with the IR coreceptors Ir8a, Ir25a, and Ir76b that might predict their functional properties. Genetic knockin and *in vivo* functional imaging of IR41c-expressing neurons indicate both odor-induced activation and inhibition in response to select amine compounds. Targeted mutagenesis of IR41c does not abolish behavioral responses to the amine compounds. Our study provides a comprehensive map of IR-expressing neurons in the main olfactory appendage of mosquitoes. These findings show organizing principles of *Anopheles* IR-expressing neurons, which might underlie their functional contribution to the detection of behaviorally relevant odors.

## INTRODUCTION

There are ~3,500 species of mosquito on earth, yet the most dangerous are the ~100 species that serve as vectors of human diseases.[1] Among these species, *Anopheles* and *Aedes* mosquitoes represent two important genera of medical health significance to humans. The process of seeking human hosts and blood feeding is a critical conduit for the transmission of pathogens by disease-carrying mosquitoes. Some members of the *Anopheles gambiae* complex, including *An. gambiae* s.s. (*An. gambiae* molecular S form) and *Anopheles coluzzii* (*An. gambiae* molecular M form),[2] are major vectors of malaria, largely because they strongly prefer to host-seek humans.[3–6] *Anopheles* rely primarily on their olfactory system to find mates, search for suitable oviposition sites, and locate blood hosts.[4] The ability to detect sensory cues is enabled by the possession of sensory receptors expressed by neurons housed in specialized sensillar hairs in the olfactory appendages—the antennae, maxillary palps, and labella.

The mosquito antenna is the main olfactory organ for detecting odors. The female *Anopheles* antenna contains 3 different types of sensilla categorized based on size and shape identified across 13 segments (flagellomeres).[7] Each sensillum in the mosquito olfactory appendages contains on average between 2 and 4 neurons that are activated by volatile odorants.[7,8] The female *An. gambiae* antenna is densely populated with ~1,500 olfactory receptor neurons, mostly housed in the trichoid sensilla.[9,10] These neurons express odor-gated sensory receptors that bind odor ligands, ultimately leading to neuronal activation.

Three main classes of odor-gated receptors have been identified in mosquitoes. The odorant receptors (ORs), which function with an obligate OR coreceptor, are found in antennal trichoid, maxillary palp capitate peg, and labella T2 sensilla. The olfactory gustatory receptors (GRs), which function as a complex to detect carbon dioxide, are found on a single neuron in maxillary palp capitate peg sensilla. The olfactory ionotropic receptors (IRs), which function with one or more IR coreceptors (IR8a, IR25a, and IR76b), reside in the antennal grooved peg sensilla, coeloconic sensilla, and possibly trichoid sensilla.[4] Among these three receptor classes, the IRs are the most ancestral with evolutionary history that differs from the ORs and GRs.[11–13]

Functionally, ORs respond to a variety of plant-derived volatiles and human skin emanations, while olfactory GRs respond to carbon dioxide and some odorants.[14–16] Mosquito IRs are responsive to acids and amines[17–19] and might be involved in human host preferences.[19] However, the functional roles of mosquito IRs extend beyond sensing behaviorally relevant odorants.[20] Several lines of evidence suggest multiple roles for insect IRs including oviposition cues detection,[21] courtship behavior,[22] thermosensation,[23–25] humidity detection,[24,26] and taste sensation.[27,28] The diverse roles of IRs remain consistent with the widespread expression pattern across insect body parts. In *Drosophila*, IRs are broadly expressed and can be detected in the legs, pharynx, labellum, and wings.[21] Transcriptomic profiling of *Aedes aegypti* mosquitoes also revealed broad expression of IRs not only in the olfactory appendages but also in the legs, rostrum, and abdominal tip.[29] Similarly, elevated IR transcripts were detected in the body of *An. gambiae* mosquitoes.[30]

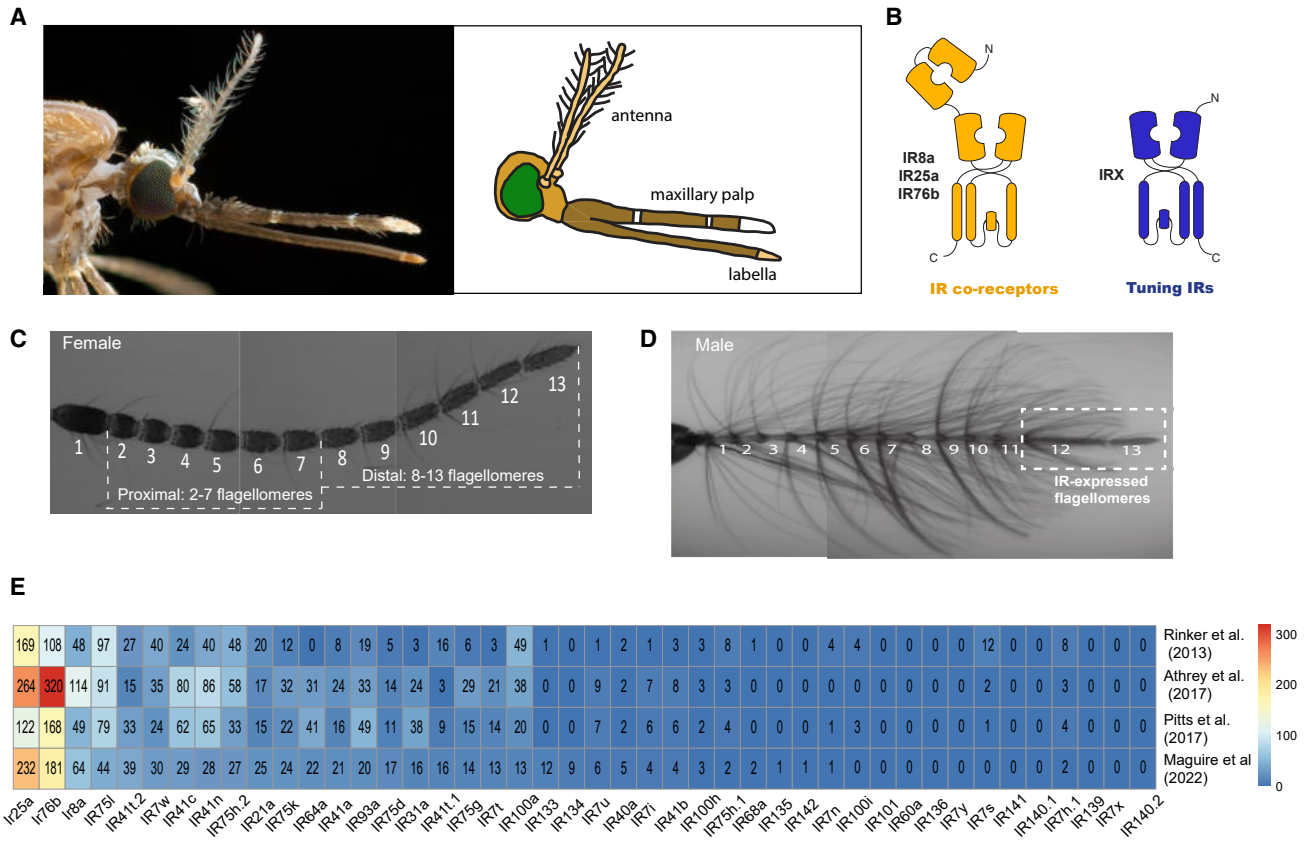


**Figure 1. Transcript abundance of ionotropic receptors in the main olfactory appendage of *Anopheles gambiae* mosquitoes**

(A) A side view of a female *Anopheles gambiae* mosquito showing the olfactory appendages (antenna, maxillary palp, and labella) involved in odor detection and taste. Licensed photo by Alex Wild.

(B) Schematic of *Anopheles* ionotropic receptors (IRs) showing the structures of IR coreceptors and tuning (odor-binding) IRs. IRs are ligand-gated ion channels capable of forming heteromeric functional complexes. Each tuning IR requires at least one or more IR coreceptors (IR8a, IR25a, and IR76b) to function.

(C) Confocal z stack images of *An. coluzzii* antenna. The numbers represent each flagellomere from the antennal base (1) to the antennal tip (13). The proximal region comprises flagellomeres 2–7, whereas flagellomeres 8–13 represent the distal region. Female antennal image showing the 13 flagellomeres grouped into proximal and distal regions.

(D) Male antennal image with the flagellomeres containing olfactory neurons marked with a dashed box.

(E) Heatmap showing the transcript levels of all IRs predicted from the *Anopheles* genome. Data are compared across four independent studies and arranged in transcript abundance order of IRs in the female antennae.

While the antennal topography of a limited number of *Anopheles* OR-positive cells has been examined,[31,32] the population and the distribution patterns of IRs in the antenna remained poorly characterized. Here, we performed hybridization chain reaction whole-mount fluorescence *in situ* hybridization (WM-FISH) of the antenna for the majority of antennal IRs, used CRISPR-Cas9 to generate a knockin of one of the most highly expressed IRs, and performed calcium imaging of this IR-expressing neuron to characterize its odor-response profile. We provide a detailed spatial antennal map of the location of IR-expressing neurons across the antennae, highlighting a global organization of some IRs into proximal and distal regions of the antenna. The abundance, spatial localization, and co-expression pattern of cells expressing a defined IR could offer insights into their functional roles and contribution to the detection of behaviorally relevant odors.

## RESULTS

### Comparative transcriptomic profiles of *An. coluzzii* IRs in the main olfactory appendage

We performed transcriptomic analysis on the female *An. coluzzii* (strain N'Gousso) antennae, the main olfactory appendage (Figure 1A). RNA sequencing (RNA-seq) data for IRs were retrieved from transcriptomic data reported from four previous studies.[30,33–35] A total of 44 IRs were predicted in the *An. gambiae* genome comprising 3 IR coreceptors and 41 tuning IRs (Figure 1B). The female antenna is morphologically different from the male antenna (Figures 1C and 1D). Although both are segmented into 13 flagellomeres, male antennae contain long (presumably mechanosensory) fibrillae bristles on flagellomeres 1–10 not present in the female. As discussed in greater detail below, we grouped the flagellomeres in the female antenna into proximal (2–7) and distal

(8–13) regions (Figure 1C). We next compared antennal transcriptome RNA-seq data across the four studies (Figure 1E). As expected, abundant expression levels for the IR coreceptors (IR8a, IR25a, and IR76b) was consistently identified (Figure 1E). A cutoff transcript level (>10 RPKM reported from at least two datasets) was set to define highly expressed IRs. Arrangement of IRs based on transcript abundance revealed the expression of 20 highly expressed IRs, whereas a total of 24 lowly expressed or undetected IRs (<10 RPKM from two or more datasets) were reported across all 4 antennal transcriptome datasets (Figure 1E). The data from Maguire et al.[34] and Rinker et al.[35] identified IR25a as the most abundant IR in the antenna. Other studies reported that IR76b transcript levels exceeded other IR coreceptors.[30,33] Interestingly, the IR75l tuning receptor transcript level was more enriched than IR8a coreceptor in two independent studies.[30,35] Differences in transcript values might be explained by differences in tissue preparation, data acquisition, or bioinformatic analysis. The IRs not abundant in antennal tissues might still be expressed in other tissues. The transcript enrichment of tuning IRs in the antenna, such as IR75l, IR41t.2, IR7w, and IR41c, might suggest an important functional role for these IRs in this main olfactory appendage.

## Spatial expression of antennal IRs revealed by fluorescence *in situ* hybridization

RNA-seq data report the abundance of an IR in bulk antennal tissues but does not reveal the location or number of the IR-expressing neurons across the antenna. For example, highly enriched antennal IR transcripts might be due to one small antennal segment (flagellomere) containing many neurons expressing an IR, to many IR-expressing neurons spread across all 13 antennal flagellomeres, or to a few IR neurons expressing high levels of the IR. To map IR-expressing neurons, we performed hybridization chain reaction WM-FISH on antennal tissue using fluorescently labeled probes of target IRs. We first performed immunostaining on the seven most abundant IRs reported from our transcriptomic data obtained from the female antennae.[34] The probes for four tuning IRs (Ir7w, Ir41c, Ir41t.2, and Ir75l) and three coreceptor IRs (Ir8a, Ir76b, and Ir25a) detected the localization of these IRs across the flagellomeres in the female and male antenna (female, Figure 2; male, Figure S1). As expected, each flagellomere of the female antennae was densely populated with IR coreceptors (Figures 2E–2G). Interestingly, spatial mapping of the abundant tuning IRs revealed differential expression across the antenna. Clusters of Ir7w-, Ir41c-, and Ir41t.2-expressing neurons were found mainly in distal flagellomeres, while Ir75l was typically found in proximal flagellomeres (Figures 2A–2D; Table S1). Statistical analysis revealed that IR coreceptors are more abundantly localized to the distal region (Figure S2A). This might reflect a higher density of IR-expressing neurons in distal flagellomeres than in proximal flagellomeres. Unlike the female antenna, IR-positive cells were all localized to the 12th and 13th flagellomeres and undetectable in proximal segments of the male antenna. The 13th flagellomere of the male antenna is more enriched with IR coreceptors than the 12th segment (Figure S2B). Consistent with the robust transcript abundance of IR coreceptors (Figure 1E), the number of cells expressing IR coreceptors exceeded the tuning IRs in the female (Figure S2C) and male (Figure S2D) antennae. Notably, IR75l-positive cells were robustly localized to the proximal region compared with the distal part ($p = 0.0003$) (Figure S3). On the other hand, we identified more cells expressing IR7w, IR41t.2, and IR41c tuning IRs in the distal region (Figure S3).

Among the highly expressed tuning IRs examined in the female antennae, IR41c-positive cells were more robustly detected compared with other tuning IRs, whereas IR41t.2-expressing cells were the most enriched tuning IR in the male antennae (Figures S2C and S2D). The abundance of IR41c-expressing cells in the female antennae could indicate their importance in detecting a crucial odor cue. The male-enriched IR41t.2 might similarly be important for male behaviors such as nectar seeking or mate finding. A comparison between the number of IR-expressing cells and transcriptomics data suggests that some IRs might be highly expressed in a small number of neurons (Table S2). For example, IR75l transcript levels were reported to be more abundant than IR8a[30,35] but the number of cells expressing IR75l is fewer compared with IR8a in both male and female antennae (Figures 1E, 2, and S2C). This suggests that IR75l might be highly expressed in a small set of neurons, while the more densely populated IR8a-positive cells express relatively lower levels of the IR8a transcript. IR93a transcripts per olfactory neuron similarly appeared high based on transcript levels and the number of IR93a-expressing neurons (Table S2).

## *Anopheles* IRs are expressed in stereotyped topographical regions across the antenna

We next generated 20 additional *in situ* probes and performed WM-FISH to map the spatial distribution for all enriched antennal-expressed IRs as reported by transcriptomic data. In addition to the proximally localized IR75l-positive cells (Figure S3), we detected additional IRs (IR41a and IR75d) that were enriched in the proximal region (Figures 3A and 3B). The majority of antennal IR-expressing cells were consistently abundant in the 12th and 13th flagellomeres of the female antenna (Figures 3A and 3B). Notably, approximately 80% of IR93a-expressing cells detected *in situ* were localized to the 13th flagellomere (Figure 3B). In a few samples, we detected the expression of IR75l and IR76b in the first flagellomere (Figure 3C). While the number of tuning IR-positive neurons per flagellomere was consistent from animal to animal, the position of these IR-positive cells within a flagellomere appeared to be more variable. Although RNA-seq data detected IR100a in the female antenna, we could not detect cells expressing IR100a by WM-FISH. It is possible that the IR100a expression level in a neuron was below the detection limit of our *in situ* protocol. Given this observation, we did not generate probes for IRs with transcript levels below IR100a.

We also analyzed the abundance of a limited set of IRs across the male antenna (Figures 3D–3F). Consistent with the unique expression pattern of IR75l in the proximal region of the female antennae, the male antenna contained IR75l-positive cells only in the 12th antennal segment, while the 13th segment was devoid of IR75l cells (Figures 3D and 3E). In general, more


**Figure 2. Topography of highly expressed IRs in the female *Anopheles coluzzii* antenna**

Whole-mount fluorescence *in situ* hybridization images of female antenna. z stack images from three different sections of the antenna were captured at 25× magnification and combined to form a single antennal image. Probes were generated for highly expressed tuning IRs: (A) IR7w, (B) IR41c, (C) IR41t.2, (D) IR75l, and IR coreceptors (E) IR8a, (F) IR76b, and (G) IR25a. The antennal region demarcated by a white dashed line is also shown magnified. The numbers added to the first panel represent the flagellomeres. The green color in the antennal images is background fluorescence. Scale bars, 100 µm.

IR-expressing neurons were localized to the distal 13th flagellomere than in the 12th flagellomere (Figures 3D and 3E). It should be noted that the abundant IRs examined here by *in situ* analyses were based on female antennal RNA-seq expression studies; male-specific antennal RNA-seq might identify a different set of abundant IRs that warrant further study.

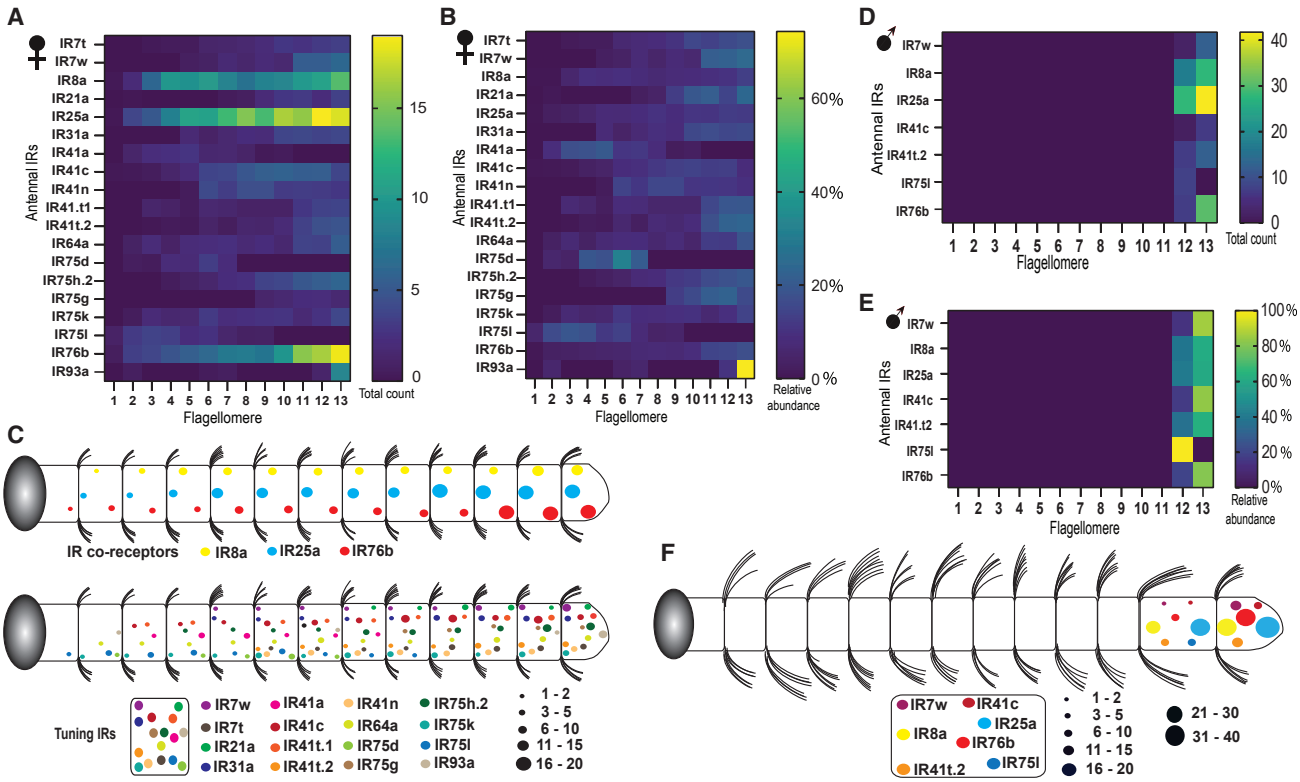


**Figure 3. A spatial map of IR expression and relative distribution in female and male antennae**

(A) Heatmap representing the number of IR-expressing cells per flagellomere in the female antenna (n = 11–14).

(B) Relative abundance of IR-positive cells across female flagellomeres (n = 11–14).

(C) Cartoon model showing the spatial map of IRs across the 13 flagellomeres.

(D) Heatmap representing the number of IR-positive cells per flagellomere in the male antenna (n = 9–14).

(E) Heatmap showing the relative abundance of IRs in a flagellomere across a male antenna (n = 9–14).

(F) A cartoon model showing a spatial map of expressed IRs in the male antenna of *An. coluzzii*. The size of the circle corresponds to the number of cells identified. Each color represents a different IR. The key serves as a reference guide to help identify the tuning IRs found in a flagellomere; it does not indicate their relative spatial position in a flagellomere.

## Multiplex immunofluorescence reveals IR co-localization patterns

Tuning IRs form a functional complex with at least one or more coreceptors,[36,37] which might influence their functional properties.[38,39] In general, the IR8a coreceptor is necessary for responses to acids while the Ir76b coreceptor is necessary for response to amines.[17,18,37,40] To examine this, we utilized two-probe WM-FISH to identify which IR coreceptors were co-expressed in the same cells as any of the four highly expressed tuning IRs. We identified the co-expression patterns of IR7w, IR41c, IR41t.2, and IR75l with coreceptors IR8a, IR25a, and IR76b (Figures 4A–4C and S4–S6; Table S3). The IR41 clade of IRs includes IR41c and IR41t.2, which showed similar co-expression patterns and did not co-label with IR8a (Figures 4A and S4). We observed partial overlap between IR7w-positive cells and IR8a-expressing cells (Figure 4A). In contrast, IR75l-expressing cells completely overlapped with IR8a-postive cells (Figure 4D). Co-localization of *An. coluzzii* IR7w and IR75l with IR8a suggests they may be tuned to acids. Notably, all four tuning IRs examined in the study completely overlap with IR25a-positive cells (Figures 4B and S5). The distinct co-expression patterns of IR41c and IR41t.2 with IR25a and IR76b, but not IR8a (Figures 4 and S4–S6), could suggest a role for these tuning IRs in the detection of amine chemical compounds.

Given the broad expression of the coreceptor IR25a, we asked if IR25a was ubiquitously expressed in all IR-positive cells. We performed multiprobe WM-FISH immunostaining for IR25a, IR76b, and IR8a to uncover the combinatorial relationship among these IR coreceptors. We focused on coreceptor co-expression in the 11th flagellomere as it is enriched for IRs yet is less densely populated compared with the 12th and 13th flagellomere; this allowed for optimized data analyses. Notably, we consistently observed that all IR76b-expressing cells also co-labeled with IR25a (Figure 5A). However, in some cells, IR25a selectively co-expressed with IR8a but not with IR76b (Figure 5A). Surprisingly, we identified some cells that were only positive for IR8a and deficient for IR25a and IR76b (Figure 5B). Some cells were exclusively labeled by IR25a and negative for IR8a and IR76b (Figure 5B). Scoring the number of IR coreceptor cells that co-express IR8a, Ir76b, and Ir25a highlighted the invariant combination of IR76b and IR25a dual labeling (Figures 5C and 5D). Altogether, our data identified various

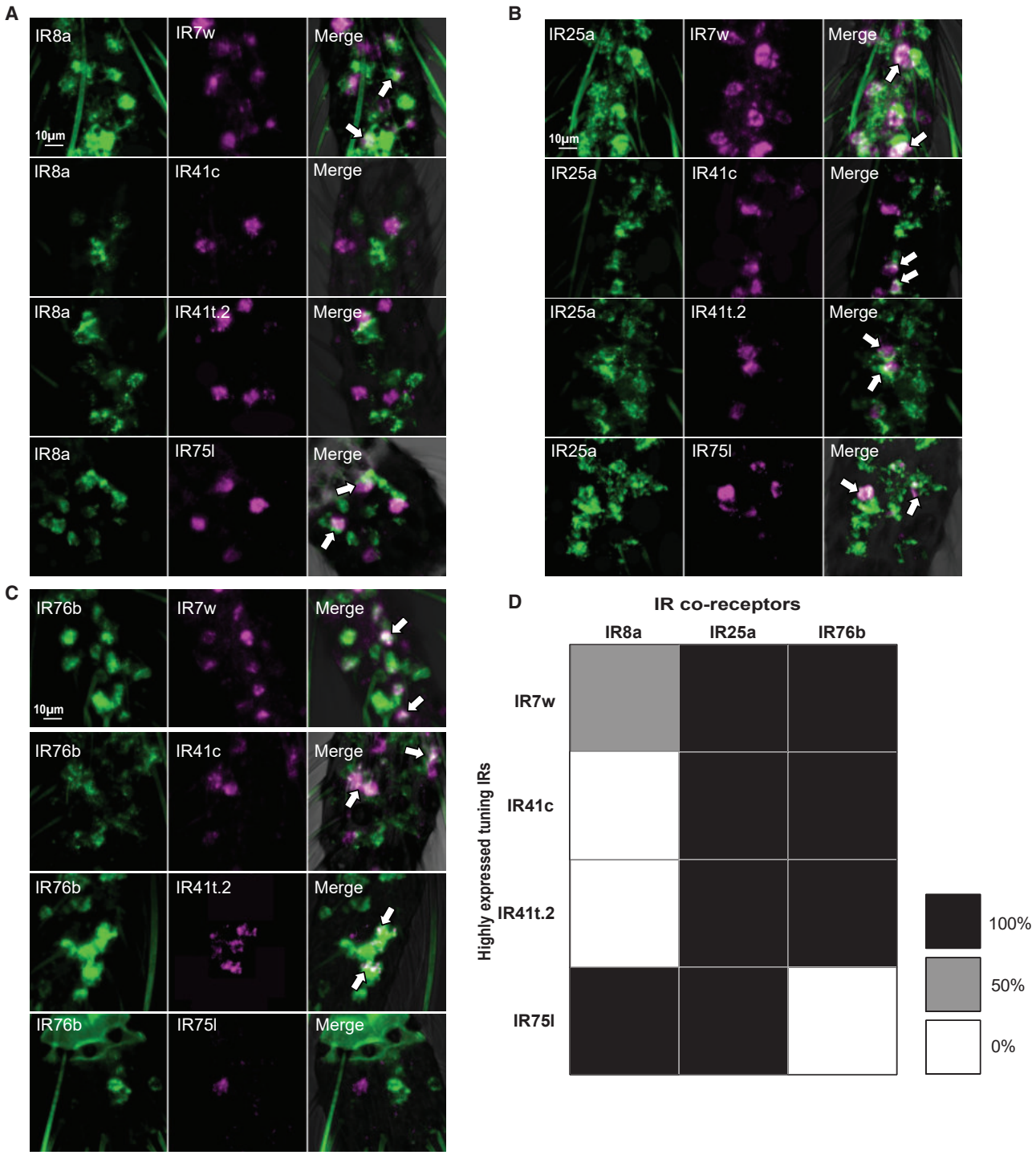


**Figure 4. Co-expression patterns of highly expressed tuning IRs with IR coreceptors**

*In situ* images showing co-localization of the four highly expressed tuning IRs with (A) IR8a, (B) IR25a, and (C) IR76b coreceptors. Tuning IR probes were conjugated to the Alexa 647 fluorophore (red) while IR coreceptor probes were linked to the Alexa 488 fluorophore (green). Arrowheads point to example co-localized cells.

(D) Summary heatmap showing the co-expression patterns of the four tuning IRs with IR coreceptors (n = 5). The percent co-expression was calculated as the percent of tuning IR-positive cells that co-labeled with the IR coreceptor(s). See Figures S4–S6 for additional examples.

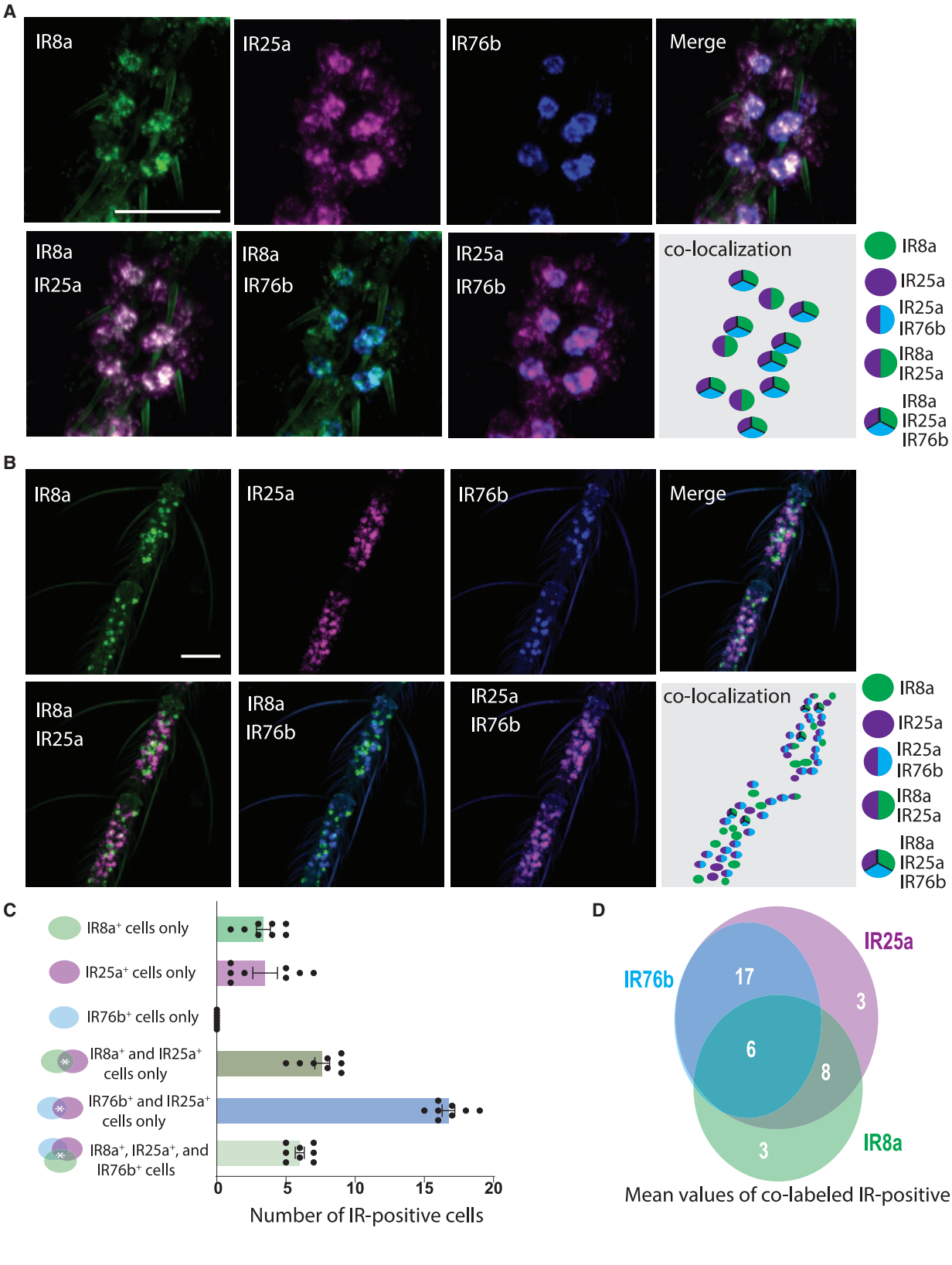


(legend on next page)

combinations of coreceptors with a small population of IR-positive cells (~8%) lacking IR25a expression.

## IR-expressing cell numbers are not modulated by blood feeding or aging

Transcriptomic evidence revealed that mRNA abundance of IRs in the mosquito antenna are modulated after a blood meal.[35] In addition, certain behavioral changes have been linked to the upregulation or downregulation of some olfactory receptors in the olfactory appendages.[35,41] We asked if blood feeding or age might alter the abundance of olfactory IR neurons as observed using WM-FISH. This might reveal the addition or subtraction of IR-expressing neurons during these different adult stages. We compared the number of IR-expressing neuron populations in actively host seeking mosquitoes, blood fed mosquitoes, and aged mosquitoes. Our data revealed no obvious changes to the number of IR-positive cells among these three mosquito stages (Table S4). It is possible that transcriptional changes in individual IR-expressing neurons might be subtle and undetectable by WM-FISH. The changes in WM-FISH signal intensities might reflect changes in IR expression in a neuron, but our WM-FISH approach makes it difficult to quantify this across different conditions. Altogether, our data suggest that previously observed transcriptional changes across adult stages was likely not caused by gross changes to the number of IR-expressing neurons in the antenna.

## Targeted CRISPR knockin and expression profiling of IR41c

IR41c-expressing cells were among the most numerous in the female antennae (Figure S2C). This suggests that odors detected by these IR41c-expressing neurons could be strong drivers of behavior. While heterologous expression of *An. gambiae* IRs in *Xenopus* oocytes for the majority of tuning IRs was non-functional, IR41c expression with IR25a and IR76b did lead to a functional IR channel.[30] In this assay, IR41c/IR25a/IR76b channels were activated by the amines 3-methylpiperidine, 3-pyrroline, and pyrrolidine.[30] The co-expression pattern we observe for IR41c with amine-sensing coreceptors IR76b and IR25a (Figures 4B and 4C) supports the *in vivo* role for IR41c neurons to detect amines. Genetic labeling and functional characterization of IR41c neurons could allow a direct comparison between endogenous neuronal responses and those identified in a heterologous system. We used the homology-assisted CRISPR knockin method[39,42] to target a *T2A-QF2* cassette 150 base pairs downstream of the start codon of the IR41c gene (Figure 6A). This approach was used to both capture the endogenous expression pattern of the IR41c gene as well as generate a loss-of-function mutation. Transgenic *IR41c-T2A-QF2* mosquitoes were outcrossed into the wild-type *Anopheles coluzzii* N'Gousso strain for six generations. We validated *IR41c-T2A-QF2* animals by PCR of the target gene and visual screening for the red fluorescent marker in the eye and ventral nerve cord of the larvae (Figure 6B).

To examine the expression pattern of the *IR41c-T2A-QF2* knockin, we crossed *IR41c-T2A-QF2* mosquitoes to mosquitoes carrying the *QUAS-CD8:GFP* reporter line.[43] In the transgenic progeny (*IR41c-T2A-QF2*; *QUAS-CD8:GFP*), QF2 drives CD8:GFP expression in all IR41c neurons. Confocal imaging of the antenna revealed GFP-labeled IR41c neurons in the antenna (Figure 6C). By performing WM-FISH on the antennae of IR41c transgenic animals, we found excellent overlap (97.76%) between the *IR41c-T2A-QF2*-induced expression and the *IR41c in situ* probe (Figure 6C; Table S5). To visualize the innervation pattern of IR41c-expressing neurons in the *An. coluzzii* brain, we dissected the brains of *IR41c-T2A-QF2*; *QUAS-CD8:GFP* animals and stained for the CD8:GFP labeled axons. We found that IR41c-expressing neurons projected to the antennal lobe and innervated a single ventral posterior glomerulus (Figure 6D). This is consistent with previous results that suggested IR-expressing neurons might primarily target posterior antennal lobe glomeruli.[43]

## *An. coluzzii* IR41c neurons are responsive to select amines

To uncover the odor compounds that activate IR41c neurons, we crossed the *IR41c-T2A-QF2* line to the calcium indicator line *QUAS-GCaMP6f*[44] and measured the odor-induced activity of IR41c-positive cells as detected by changes in fluorescence before and after odor delivery (Figure 7A). Odor response was analyzed by profiling the short-term and long-term activation of the neurons (Figure 7B; see methods for details). We established a transheterozygous line (*IR41c-T2A-QF2*/+; *QUAS-GCaMP6f*/+) that has a functional copy of IR41c, and a homozygous mutant line (*IR41c-T2A-QF2*/*IR41c-T2A-QF2*; *QUAS-GCaMP6f*/*QUAS-GCaMP6f*). We identified dual excitatory and inhibitory responses of IR41c neurons in the transheterozygous line to select amines but not to repellents or carboxylic acids (Figures 7C–7F and S7A). The amine 3-pyrroline exhibited the strongest activation of IR41c neurons (Figures 7C and S7B). In contrast, the amine 2-acetylpyridine elicited robust inhibition of IR41c neurons (Figures 7D and S7C). Notably, pyrrolidine exhibited a combination of a short-term inhibitory response followed by a long-term excitatory response (Figures 7E and S7D). The observed excitatory and inhibitory responses suggest IR41c-expressing neurons can utilize a large dynamic range when responding to amines. Interestingly, we observed fewer IR41c-expressing neurons in the mutant line than in the transheterozygote. This may suggest that mutation of IR41c could lead to neuronal loss. In the few IR41c-expressing neurons remaining

**Figure 5. IR coreceptor co-expression analyses**

(A) WM-FISH immunostaining of IR8a (green), IR25a (magenta), and IR76b (blue) coreceptors in flagellomere 11.

(B) WM-FISH immunostaining of IR8a (green), IR25a (magenta), and IR76b (blue) coreceptors in flagellomeres 10 and 11. The cartoon for co-localization represents the cells in the "merge" panel.

(C) Bar chart summarizing the different IR-positive cell populations identified in the 11th flagellomere from 8 animals.

(D) Venn diagram illustrating the mean number of co-labeled IR-positive cells in the 11th flagellomere from 8 animals. Mean values were rounded to the nearest whole number. Scale bars, 10 μm.

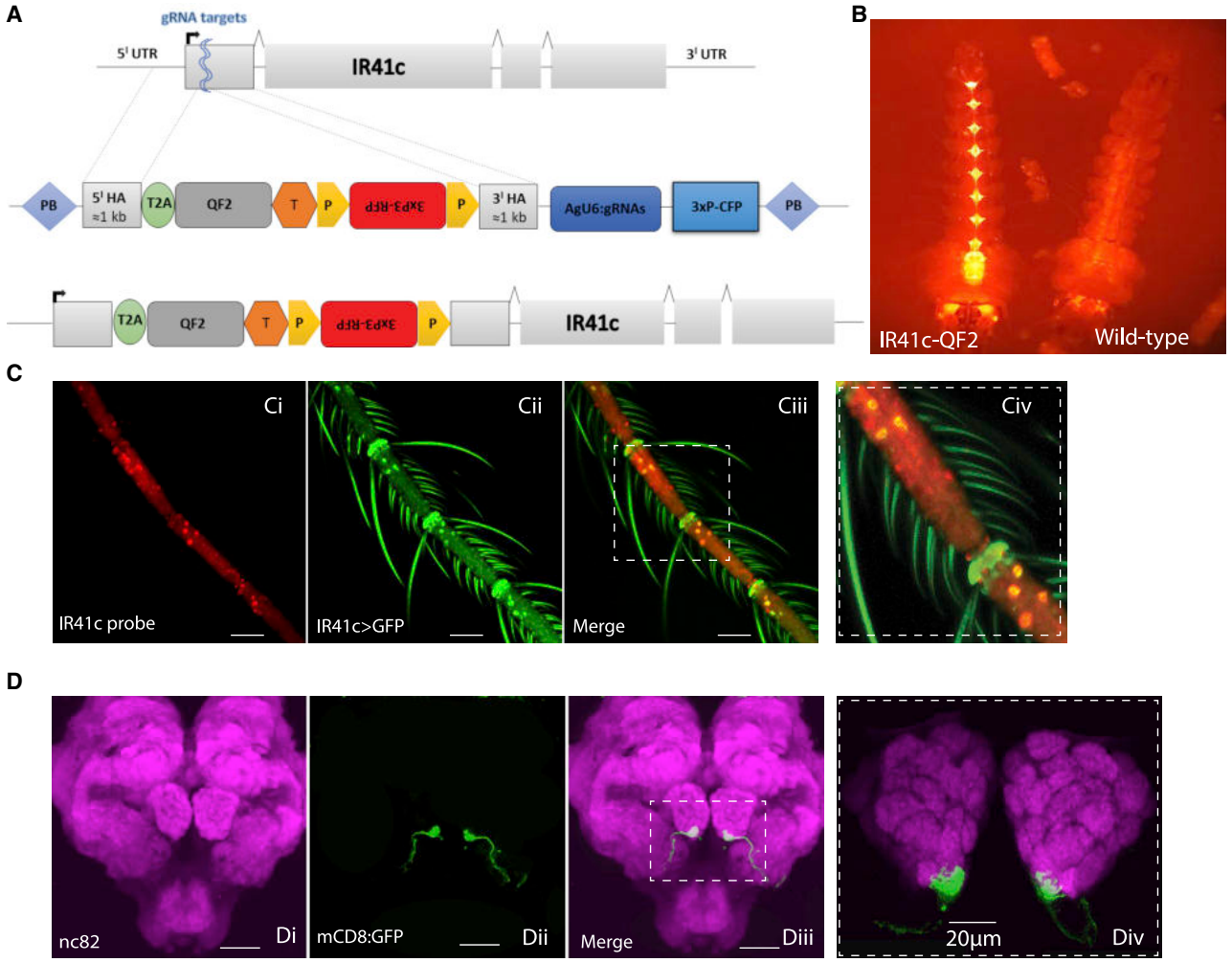


**Figure 6. Targeted mutagenesis and neuron expression profiling of tuning IR41c**

(A) Cartoon model showing the genetic HACK construct targeting *T2A-QF2* into the first exon, 150 base pairs downstream of the ATG start codon for IR41c. The guide RNA (gRNA) targets are flanked by 5′ homology arm (HA) and 3′ HA homologous to the IR41c gene. The letter "T" indicates the transcriptional terminator for the polycistronic *IR41c-T2A-QF2* mRNA. The T2A ribosomal skipper allows the translation of a single transcript into two protein products (a truncated IR41c-T2A and QF2). Included in the cassette is a *3XP3-RFP* selection marker (mCherry) to fluorescently label the transgenic line. Flanked by the selection marker are *loxP* sites (P). Outside the homology arms, the *An. gambiae* RNA polymerase III *U6* promoter drives expression of gRNAs. These gRNAs will not be incorporated into the knockin.

(B) Image showing *IR41c-T2A-QF2* transgenic larvae marked with a red fluorescently labeled protein in the eye and ventral nerve cord. For comparison, wild-type larvae show only autofluorescence.

(C) (Ci) Immunostaining of female antenna with IR41c probes conjugated to Alexa 647 to label IR41c-expressing cells (red). (Cii) Confocal antenna image of IR41c knockin lines driving the CD8:GFP reporter. This is a wet mount of the antenna without immunostaining. (Ciii) Co-labeling of IR41c probes and *IR41c-T2A-QF2* driving GFP. The IR41C knockin line faithfully recapitulates IR41c gene expression patterns as detected by *in situ*. (Civ) Magnified image of the area marked in (Ciii).

(D) (Di) Whole-brain immunofluorescence of female *An. coluzzii* stained with the Bruchpilot antibody nc82, a synaptic marker that labels brain neuropil. (Dii) IR41c neurons extend axons from the antennae and innervate the antennal lobe. (Diii) Merge of images (Di and Dii). (Div) Image of (Diii) captured at 60× magnification. Scale bars, 50 μm (unless otherwise specified).

at 2–3 days post eclosion in the IR41c mutant, we did not detect any odor-evoked activity (Table S6).

We further questioned if the loss of IR41c might result in observable changes to olfactory behaviors. We observed that the amine compounds found to activate IR41c neurons (3-pyrroline, 2-acetylpyridine, pyrrole, and pyrrolidine) directed repulsive behaviors when tested in the close proximity response assay[44] (Figure 7G). We next tested the response of the *IR41c* mutant toward these odors and found no behavioral differences between mutant mosquitoes lacking *IR41c* and the wild-type control ($p = 0.1685$; Figure 7H). This suggests the loss of IR41c function was not sufficient to alter the behavioral response to amines in this assay, suggesting that other olfactory neurons might be acting redundantly to mediate responses to these amines.

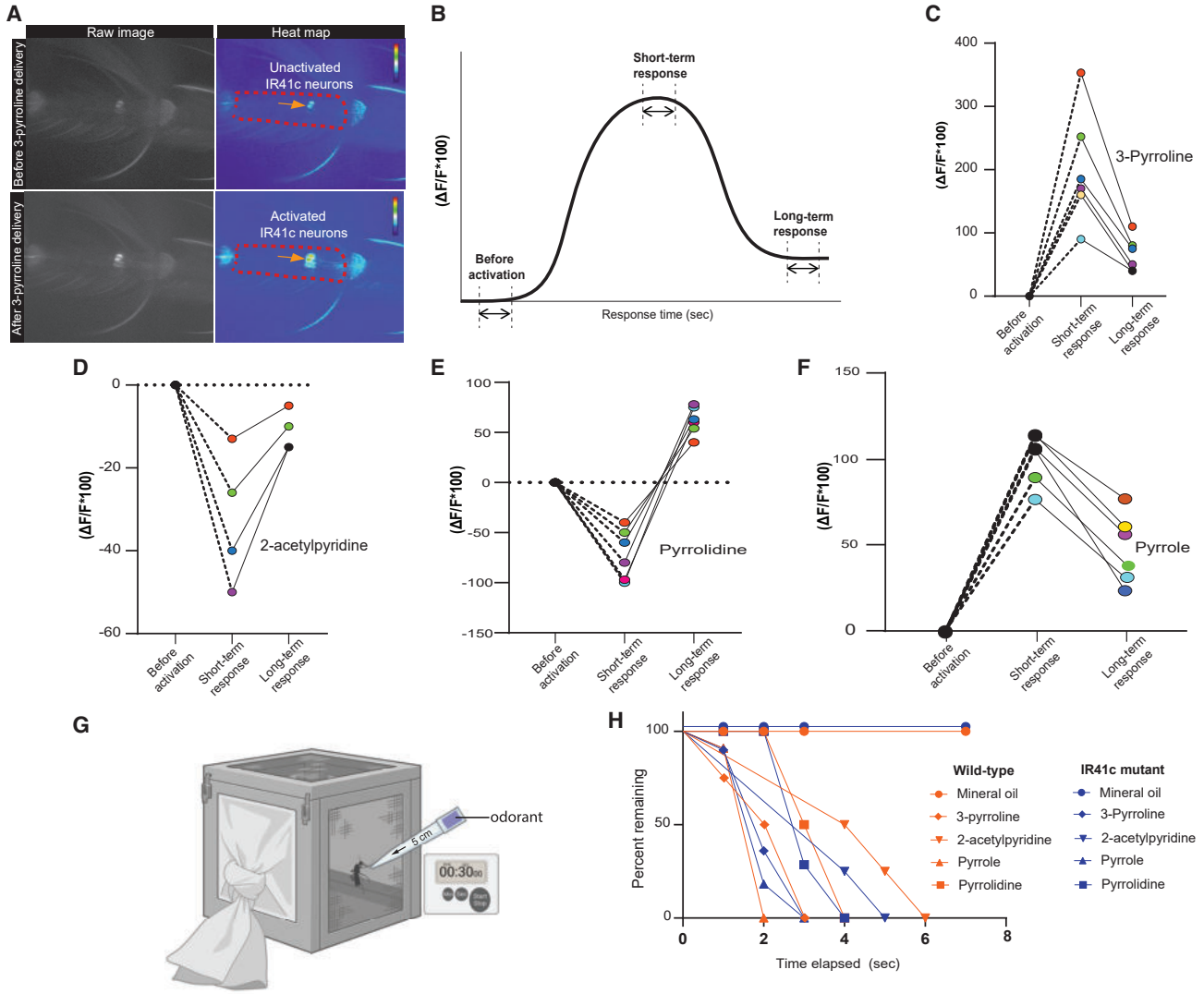


**Figure 7. Odor response profiles for *An. coluzzii* IR41c-expressing neurons**

(A) Example calcium imaging response of IR41c-expressing neurons toward 3-pyrroline. Genotype: *IR41c-T2A-QF2*, *QUAS-GCaMP6f*.

(B) Schematic defining short-term and long-term responses. Change in fluorescence before activation was determined by averaging responses from frames 20–40 before odor delivery at frame 50. This corresponds to 4–8 s before the odor stimulus at the 10 s mark. A short-term response was estimated by averaging the 10 frames (2 s) surrounding the maximum activation or inhibition in response to the odor pulse. A long-term response was estimated from frames 80–100 (corresponding to 16–20 s). Neuronal activities did not return to basal fluorescence even after 100 frames (20 s) for all odors tested.

(C–F) Quantification of short-term and long-term odor-evoked response elicited by IR41c neurons to select amines, including (C) 3-pyrroline (n = 6), (D) 2-acetylpyridine (n = 4), (E) pyrrolidine (n = 6), and (F) pyrrole (n = 6). Different colors represent different IR41c-positive cells examined in different animals.

(G) Close proximity response behavioral assay.

(H) Results obtained from the close proximity response assay. The curve shows the time elapsed before wild-type mosquitoes and *IR41c* mutant mosquitoes (n = 4–7) flew away after being approached by an odorant. Odors were tested at 1% concentration. Data were analyzed by Kaplan-Meier simple survival analysis followed by log rank test for trend. There was no significant difference between response to odor treatment in the wild-type and IR41c mutant (p = 0.6814).

## DISCUSSION

We present here a comprehensive spatial map of IR-expressing neurons across the entire *Anopheles* antenna. The majority of IRs were most abundant in the distal flagellomere in both female and male mosquitoes (Figure 3), suggesting the distal flagellomere to be the most sensitive region for detecting volatile cues. Nonetheless, we also identified IRs whose expressing neurons were primarily localized only to proximal (IR41a, IR75d, and IR75l) or distal (IR7w, IR21a, IR41n, IR41.t2, IR75g, and IR93a) antennal flagellomeres. These data suggest an additional level of organization may exist separating the antenna into proximal and distal domains. If these domains similarly reflect discrete olfactory signaling domains remains to be explored.

Of the 44 IRs identified in the *Anopheles* genome, nearly half had elevated transcript levels in the antenna. Bulk antennal RNA-seq data suggest weak transcript expression for some of these tuning IRs; however, we could not detect neurons expressing these IRs by *in situ* hybridization. This might reflect differences in the sensitivity of these two approaches. RNA-seq, as a bulk measure, might be able to identify IR transcripts that are weakly expressed across many neurons, whereas such low expression of IR transcripts per neuron might be below the level of detection of our *in situ* method. Alternatively, RNA-seq might be able to identify IRs expressed in small neuronal populations resistant to the *in situ* protocol.

## The flagellomere as an organizing antennal unit of IRs in the *Anopheles* antennae

By mapping the majority of tuning IRs to neurons across many antennae, we can reveal if patterns of neuron organization exist within a flagellomere. We observed that the number of IR-expressing cells appeared stereotyped from antenna to antenna; that is, the same number of tuning IR-expressing neurons were consistently found across many samples. Interestingly, the exact position of an IR-expressing neuron within a flagellomere was variable. This suggests that the flagellomere is an organizing unit for olfactory neurons, but that olfactory neurons do not occupy fixed locations within each flagellomere.

A neuron might be able to increase its sensitivity to sensory cues by increasing expression of its tuning IR receptor. While it remains to be determined if transcript levels directly relate to protein abundance, our work identified a couple of IR-expressing neurons that appear to be highly expressed. IR75l and IR93a appear to be at least 2-fold more highly expressed in their respective neurons compared with other IRs. IR93a has been linked to temperature and humidity sensing in *Drosophila* and *Anopheles*,[24,26] and an increased abundance might be required to mediate this affect. The functional role for IR75l remains to be determined. It also remains possible that additional antennal neurons express these IR receptors at levels below the detection of our *in situ* analyses.

Transcriptomics analyses suggest that mosquito olfactory receptor expression might change as an animal continues to age or after behavioral events such as blood feeding.[45,46] Recent work examining *An. coluzzii* ORs suggest that changes in OR expression between 1 and 8 days after pupal eclosion might reflect changes to the number of neurons expressing a particular OR.[34] Such changes in olfactory receptor expression might be a mechanism to guide olfactory behaviors. We used WM-FISH to examine changes to the numbers of neurons expressing IRs after blood feeding or in aged mosquitoes (Table S2). We did not observe obvious changes to IR-expressing numbers using this method. The changes to IR expression observed by previous transcriptomics studies might reflect cumulative small changes in expression among a large population of cells that were below detection of the WM-FISH method. Our *in situ* results suggest that dramatic changes to the number of neurons that express one IR versus another is likely not utilized by *Anopheles* mosquitoes to alter olfactory responses. Nonetheless, small changes in IR expression might still be important drivers of behavior if they can evoke changes to neuronal responses.

## Combinatorial co-expression patterns of *Anopheles* IRs offer functional insights

The function of a tuning IR toward amines or acids can often be predicted by the IR coreceptor with which it complexes. Functional analysis showed that IR64a is an acid tuning receptor that forms a functional complex with IR8a to elicit acid-evoked responses.[37] Immunoprecipitation and immunostaining of *Drosophila* IR64a and the IR8a coreceptor protein further revealed that both receptors physically interact and co-express.[37] In *Ae. aegypti*, IR8a is required for detecting carboxylic acids.[17] *Drosophila* IR76b functions alongside IR25a as coreceptors necessary for amine detection.[40] Similarly, *An. coluzzii* IR76b functions as a coreceptor in neurons responsive to amines.[18] In *Anopheles* larvae, RNAi-mediated silencing of IR76b caused impaired response to butylamine.[41] These data suggest that IR co-expression with IR8a may elicit responses toward acids, whereas co-expression with IR76b suggests a functional response toward amines.

By *in situ* analyses, we found IR41c-expressing neurons to co-localize with IR25a and IR76b, but not IR8a, suggesting that IR41c might function *in vivo* to respond to amines. Indeed, we showed by calcium imaging that IR41c neurons were activated by pyrroles, a chemical class of amine compounds. A panel of carboxylic acids did not activate IR41c neurons consistent with its lack of co-expression with the acid coreceptor IR8a. The exclusive co-expression of IR75l with the IR8a coreceptor suggests it will play a role in detecting acids. The combinatorial co-expression patterns of the three IR coreceptors with the highly expressed tuning IRs further support the premise that a tuning IR requires one or more IR coreceptors to form a functional unit.[36] Given the broad expression profile of IR25a compared with other IR coreceptors, it could be assumed that all IR-positive cells would express IR25a. Interestingly, we identified cells that are IR8a positive but lack IR25a. These IR8a-positive cells might express tuning IRs narrowly tuned to carboxylic acids. All IR76b cells identified in the assay were also labeled by IR25a; this distinct co-expression pattern validates their coordinated interaction with tuning IRs to elicit amine responses.[40] We also identified some cells that express IR25a but not IR76b or IR8a; these sub-population of cells might play non-chemosensory roles in thermosensation or hygrosensation.[24]

## Mapping IR41c expression and function

Electrophysiological recordings of odor-evoked response in *Xenopus* oocytes co-injected with cRNA encoding IR41c, IR25a, and IR76b showed inward current amplitudes to few amine compounds.[30] By performing *in vivo* calcium imaging of IR41c-expressing neurons, we similarly found responses of these neurons to some amines (Figure 7; Table S6). IR41c-expressing neurons were not activated by acids, alcohol, or some amine-derived compounds such as butylamine and 3-methyl piperidine. This observation suggests IR41c neurons are narrowly tuned to a unique subset of the amine chemical class.

The ability to genetically label IR41c-expressing neurons allowed us to examine the innervation pattern of these neurons into the antennal lobe. If IR41c was expressed in multiple different olfactory neurons (possibly co-expressed with other

tuning IRs), the IR41c-labeled neurons might then target multiple antennal lobe glomeruli (reflecting multiple distinct populations of IR41c-expressing olfactory neurons). Instead, we found that the axonal projection of IR41c neurons targeted only a single ventral posterior glomerulus in the antennal lobe. This suggests that IR41c receptors are likely expressed in only one type of IR-expressing neuron. The abundance of IR41c and IR41c-expressing neurons in the *Anopheles* antenna suggests that it might be playing a critical role in the mosquito's olfactory behavior. We observed that the amines that activate IR41c-expressing neurons can mediate repulsion; however, the ethologically relevant olfactory behaviors mediated by IR41c remain to be determined.

While the response profile of IR41c-expressing neurons was mostly consistent with heterologous expression studies of IR41c, an inhibitory neuronal response of these neurons toward 2-acetylpyridine and pyrrolidine was unexpected. In addition, the initial inhibitory response to pyrrolidine was followed by activation of the IR41c-expressing neurons. The molecular mechanism underlying such inhibitory responses mediated by an IR complex is currently unknown. Interestingly, a study of *Anopheles IR76b* mutants revealed increased amine-evoked neuronal firing compared with the wild type, suggesting that IR76b could be acting in an inhibitory receptor complex.[18] Whether IR41c functions with IR76b to mediate this inhibition remains to be determined. Nonetheless, the observed excitatory and inhibitory responses in the IR41c-expressing cells could be used by the peripheral olfactory system to expand the odor-coding abilities possible from an olfactory receptor.[47]

### Limitations of the study

The WM-FISH method used to map IR-expressing neurons has its limitations. We cannot completely rule out differences in detection posed by probe penetration or by the relative hybridization rates of the probes. For example, it is possible that the most proximal antennal flagellomeres are more resistant to probe access due to densely packed fibers.[48] RNA-seq studies on these distinct regions of the antennal appendage or neurogenetic identification of IR sensory neurons[49] would help clarify if IRs are present in these antennal segments. Furthermore, quantifying the fluorescent intensity of the IR-positive cells and correlating these data to infer the abundance of RNA transcripts in each cell was not feasible. The non-uniformity in the spatial arrangement of the neurons in the antenna could also introduce some bias in the fluorescence intensity measurements. There could also be detection variability in different sample batches as the assay design cannot accommodate simultaneous treatment of all 20 different IRs. This limitation might be overcome by recent imaging technologies such as spatial transcriptomics.[50] The average number of IR transcript per neuron estimated in Table S2 is further challenged by the variability in transcriptomic data reported from the four independent studies and the efficiency of the FISH probes. While the number of IR-positive cells revealed by WM-FISH may not completely recapitulate IR native expression, our data suggest that WM-FISH offers a reliable proxy for estimating IR populations (Figure 6C).

We propose that the functional odor properties of a tuning IR could be predicted based on the co-expression pattern it shares with IR coreceptors. We examined this in only a single case. While the *in vivo* function of IR41c-expressing neurons to respond to amines was indeed predicted by its co-expression with Ir25a/Ir76b, it remains to be determined if such functional predictions can be extended to other tuning IRs.

## STAR★METHODS

Detailed methods are provided in the online version of this paper and include the following:

- KEY RESOURCES TABLE
- RESOURCE AVAILABILITY
  - Lead contact
  - Materials availability
  - Data and code availability
- EXPERIMENTAL MODEL AND SUBJECT DETAILS
- METHOD DETAILS
  - Hybridization chain reaction whole-mount fluorescence *in situ* hybridization (WM-FISH)
  - Data acquisition
  - Establishment of transgenic strains
  - Immunohistochemistry
  - Confocal microscopy
  - Calcium imaging
  - Close proximity response assay
- QUANTIFICATION AND STATISTICAL ANALYSIS

### SUPPLEMENTAL INFORMATION

Supplemental information can be found online at https://doi.org/10.1016/j.celrep.2023.112101.

### ACKNOWLEDGMENTS

We thank Chun-Chieh Lin and Darya Task for providing the *pHACK-QF2-AgU6* plasmid. We thank Ali Afify for advice on calcium imaging, as well as all the members of Potter lab for helpful discussions. This work was supported by grants from the National Institutes of Health (NIAID R01AI137078) to C.J.P., the Department of Defense (W81XWH-18-1-0732) to C.J.P.; an HHMI Hanna Gray fellowship to J.I.R., a Johns Hopkins Postdoctoral Accelerator Award to J.I.R., as well as a Johns Hopkins Malaria Research Institute Postdoctoral Fellowship to J.I.R.; and a Natural Science and Engineering Research Council Postdoctoral Fellowship to J.K.K.. We thank the Johns Hopkins Malaria Research Institute and Bloomberg Philanthropies for their support.

### AUTHOR CONTRIBUTIONS

J.I.R. performed the experiments and analyzed the data. J.I.R. and J.K.K. produced the transgenic mosquito line. J.I.R. and C.J.P. wrote the manuscript with input from J.K.K. Funding acquisition and supervision by C.J.P.

### DECLARATION OF INTERESTS

The authors declare no competing interests.

### INCLUSION AND DIVERSITY

We support inclusive, diverse, and equitable conduct of research.

Received: October 4, 2022
Revised: December 22, 2022
Accepted: January 26, 2023

## REFERENCES


1. Harbach, R.E. (2007). The Culicidae (Diptera): a review of taxonomy, classification and phylogeny. Zootaxa *1668*, 591–638. https://doi.org/10.11646/zootaxa.1668.1.28.
2. Coetzee, M., Craig, M., and le Sueur, D. (2000). Distribution of African malaria mosquitoes belonging to the Anopheles gambiae complex. Parasitol. Today *16*, 74–77. https://doi.org/10.1016/s0169-4758(99)01563-x.
3. Coutinho-Abreu, I.V., Riffell, J.A., and Akbari, O.S. (2022). Human attractive cues and mosquito host-seeking behavior. Trends Parasitol. *38*, 246–264. https://doi.org/10.1016/j.pt.2021.09.012.
4. Konopka, J.K., Task, D., Afify, A., Raji, J., Deibel, K., Maguire, S., Lawrence, R., and Potter, C.J. (2021). Olfaction in Anopheles mosquitoes. Chem. Senses *46*, bjab021. https://doi.org/10.1093/chemse/bjab021.
5. Raji, J.I., and DeGennaro, M. (2017). Genetic analysis of mosquito detection of humans. Curr. Opin. Insect Sci. *20*, 34–38. https://doi.org/10.1016/j.cois.2017.03.003.
6. Zwiebel, L.J., and Takken, W. (2004). Olfactory regulation of mosquito–host interactions. Insect Biochem. Mol. Biol. *34*, 645–652. https://doi.org/10.1016/j.ibmb.2004.03.017.
7. McIver, S.B. (1982). Sensilla mosquitoes (Diptera: Culicidae). J. Med. Entomol. *19*, 489–535. https://doi.org/10.1093/jmedent/19.5.489.
8. Kwon, H.-W., Lu, T., Rützler, M., and Zwiebel, L.J. (2006). Olfactory responses in a gustatory organ of the malaria vector mosquito Anopheles gambiae. Proc. Natl. Acad. Sci. USA. *103*, 13526–13531. https://doi.org/10.1073/pnas.0601107103.
9. Pitts, R.J., and Zwiebel, L.J. (2006). Antennal sensilla of two female anopheline sibling species with differing host ranges. Malar. J. *5*, 26. https://doi.org/10.1186/1475-2875-5-26.
10. Qiu, Y.T., Smallegange, R.C., Van Loon, J.J.A., Ter Braak, C.J.F., and Takken, W. (2006). Interindividual variation in the attractiveness of human odours to the malaria mosquito Anopheles gambiae s. s. Med. Vet. Entomol. *20*, 280–287. https://doi.org/10.1111/j.1365-2915.2006.00627.x.
11. Benton, R., Vannice, K.S., Gomez-Diaz, C., and Vosshall, L.B. (2009). Variant ionotropic glutamate receptors as chemosensory receptors in Drosophila. Cell *136*, 149–162. https://doi.org/10.1016/j.cell.2008.12.001.
12. Croset, V., Rytz, R., Cummins, S.F., Budd, A., Brawand, D., Kaessmann, H., Gibson, T.J., and Benton, R. (2010). Ancient protostome origin of chemosensory ionotropic glutamate receptors and the evolution of insect taste and olfaction. PLoS Genet. *6*, e1001064. https://doi.org/10.1371/journal.pgen.1001064.
13. Rytz, R., Croset, V., and Benton, R. (2013). Ionotropic Receptors (IRs): chemosensory ionotropic glutamate receptors in Drosophila and beyond. Insect Biochem. Mol. Biol. *43*, 888–897. https://doi.org/10.1016/j.ibmb.2013.02.007.
14. Carey, A.F., Wang, G., Su, C.-Y., Zwiebel, L.J., and Carlson, J.R. (2010). Odorant reception in the malaria mosquito Anopheles gambiae. Nature *464*, 66–71. https://doi.org/10.1038/nature08834.
15. Hallem, E.A., Dahanukar, A., and Carlson, J.R. (2006). Insect odor and taste receptors. Annu. Rev. Entomol. *51*, 113–135. https://doi.org/10.1146/annurev.ento.51.051705.113646.
16. Turner, S.L., Li, N., Guda, T., Githure, J., Cardé, R.T., and Ray, A. (2011). Ultra-prolonged activation of CO2-sensing neurons disorients mosquitoes. Nature *474*, 87–91. https://doi.org/10.1038/nature10081.
17. Raji, J.I., Melo, N., Castillo, J.S., Gonzalez, S., Saldana, V., Stensmyr, M.C., and DeGennaro, M. (2019). Aedes aegypti mosquitoes detect acidic volatiles found in human odor using the IR8a pathway. Curr. Biol. *29*, 1253–1262.e7. https://doi.org/10.1016/j.cub.2019.02.045.
18. Ye, Z., Liu, F., Sun, H., Ferguson, S.T., Baker, A., Ochieng, S.A., and Zwiebel, L.J. (2022). Discrete roles of Ir76b ionotropic coreceptor impact olfaction, blood feeding, and mating in the malaria vector mosquito Anopheles coluzzii. Proc. Natl. Acad. Sci. USA. *119*, e2112385119. https://doi.org/10.1073/pnas.2112385119.
19. De Obaldia, M.E., Morita, T., Dedmon, L.C., Boehmler, D.J., Jiang, C.S., Zeledon, E.V., Cross, J.R., and Vosshall, L.B. (2022). Differential mosquito attraction to humans is associated with skin-derived carboxylic acid levels. Cell *185*, 4099–4116.e13. https://doi.org/10.1016/j.cell.2022.09.034.
20. Raji, J.I., and Potter, C.J. (2022). Chemosensory ionotropic receptors in human host-seeking mosquitoes. Curr. Opin. Insect Sci. *54*, 100967. https://doi.org/10.1016/j.cois.2022.100967.
21. Koh, T.-W., He, Z., Gorur-Shandilya, S., Menuz, K., Larter, N.K., Stewart, S., and Carlson, J.R. (2014). The Drosophila IR20a clade of ionotropic receptors are candidate taste and pheromone receptors. Neuron *83*, 850–865. https://doi.org/10.1016/j.neuron.2014.07.012.
22. Grosjean, Y., Rytz, R., Farine, J.-P., Abuin, L., Cortot, J., Jefferis, G.S.X.E., and Benton, R. (2011). An olfactory receptor for food-derived odours promotes male courtship in Drosophila. Nature *478*, 236–240. https://doi.org/10.1038/nature10428.
23. Greppi, C., Laursen, W.J., Budelli, G., Chang, E.C., Daniels, A.M., van Giesen, L., Smidler, A.L., Catteruccia, F., and Garrity, P.A. (2020). Mosquito heat seeking is driven by an ancestral cooling receptor. Science *367*, 681–684. https://doi.org/10.1126/science.aay9847.
24. Laursen, W.J., Budelli, G., Tang, R., Chang, E.C., Busby, R., Shankar, S., Gerber, R., Greppi, C., Albuquerque, R., and Garrity, P.A. (2023). Humidity sensors that alert mosquitoes to nearby hosts and egg-laying sites. Neuron, 01122–01129.
25. Ni, L., Klein, M., Svec, K.V., Budelli, G., Chang, E.C., Ferrer, A.J., Benton, R., Samuel, A.D., and Garrity, P.A. (2016). The Ionotropic Receptors IR21a and IR25a mediate cool sensing in Drosophila. Elife *5*, e13254. https://doi.org/10.7554/eLife.13254.
26. Knecht, Z.A., Silbering, A.F., Ni, L., Klein, M., Budelli, G., Bell, R., Abuin, L., Ferrer, A.J., Samuel, A.D., Benton, R., and Garrity, P.A. (2016). Distinct combinations of variant ionotropic glutamate receptors mediate thermosensation and hygrosensation in Drosophila. Elife *5*, e17879. https://doi.org/10.7554/eLife.17879.
27. Hussain, A., Zhang, M., Üçpunar, H.K., Svensson, T., Quillery, E., Gompel, N., Ignell, R., and Grunwald Kadow, I.C. (2016). Ionotropic chemosensory receptors mediate the taste and smell of polyamines. PLoS Biol. *14*, e1002454. https://doi.org/10.1371/journal.pbio.1002454.
28. Zhang, Y.V., Ni, J., and Montell, C. (2013). The molecular basis for attractive salt taste coding in Drosophila. Science *340*, 1334–1338. https://doi.org/10.1126/science.1234133.
29. Matthews, B.J., McBride, C.S., DeGennaro, M., Despo, O., and Vosshall, L.B. (2016). The neurotranscriptome of the Aedes aegypti mosquito. BMC Genom. *17*, 32. https://doi.org/10.1186/s12864-015-2239-0.
30. Pitts, R.J., Derryberry, S.L., Zhang, Z., and Zwiebel, L.J. (2017). Variant ionotropic receptors in the malaria vector mosquito Anopheles gambiae tuned to amines and carboxylic acids. Sci. Rep. *7*, 40297. https://doi.org/10.1038/srep40297.
31. Schultze, A., Pregitzer, P., Walter, M.F., Woods, D.F., Marinotti, O., Breer, H., and Krieger, J. (2013). The Co-expression pattern of odorant binding proteins and olfactory receptors identify distinct trichoid sensilla on the antenna of the malaria mosquito Anopheles gambiae. PLoS One *8*, e69412. https://doi.org/10.1371/journal.pone.0069412.
32. Schymura, D., Forstner, M., Schultze, A., Kröber, T., Swevers, L., Iatrou, K., and Krieger, J. (2010). Antennal expression pattern of two olfactory receptors and an odorant binding protein implicated in host odor detection by the malaria vector *Anopheles gambiae*. Int. J. Biol. Sci. *6*, 614–626. https://doi.org/10.7150/ijbs.6.614.
33. Athrey, G., Cosme, L.V., Popkin-Hall, Z., Pathikonda, S., Takken, W., and Slotman, M.A. (2017). Chemosensory gene expression in olfactory organs of the anthropophilic Anopheles coluzzii and zoophilic Anopheles quadriannulatus. BMC Genom. *18*, 751. https://doi.org/10.1186/s12864-017-4122-7.
34. Maguire, S.E., Afify, A., Goff, L.A., and Potter, C.J. (2022). Odorant-receptor-mediated regulation of chemosensory gene expression in the malaria

mosquito Anopheles gambiae. Cell Rep. *38*, 110494. https://doi.org/10.1016/j.celrep.2022.110494.

35. Rinker, D.C., Zhou, X., Pitts, R.J., AGC Consortium; Rokas, A., and Zwiebel, L.J. (2013). Antennal transcriptome profiles of anopheline mosquitoes reveal human host olfactory specialization in Anopheles gambiae. BMC Genom. *14*, 749. https://doi.org/10.1186/1471-2164-14-749.
36. Abuin, L., Bargeton, B., Ulbrich, M.H., Isacoff, E.Y., Kellenberger, S., and Benton, R. (2011). Functional architecture of olfactory ionotropic glutamate receptors. Neuron *69*, 44–60. https://doi.org/10.1016/j.neuron.2010.11.042.
37. Ai, M., Min, S., Grosjean, Y., Leblanc, C., Bell, R., Benton, R., and Suh, G.S.B. (2010). Acid sensing by the Drosophila olfactory system. Nature *468*, 691–695. https://doi.org/10.1038/nature09537.
38. Herre, M., Goldman, O.V., Lu, T.-C., Caballero-Vidal, G., Qi, Y., Gilbert, Z.N., Gong, Z., Morita, T., Rahiel, S., Ghaninia, M., et al. (2022). Non-canonical odor coding in the mosquito. Cell *185*, 3104–3123.e28. https://doi.org/10.1016/j.cell.2022.07.024.
39. Task, D., Lin, C.-C., Vulpe, A., Afify, A., Ballou, S., Brbic, M., Schlegel, P., Raji, J., Jefferis, G., Li, H., et al. (2022). Chemoreceptor co-expression in Drosophila melanogaster olfactory neurons. Elife *11*, e72599. https://doi.org/10.7554/eLife.72599.
40. Vulpe, A., and Menuz, K. (2021). Ir76b is a Co-receptor for amine responses in Drosophila olfactory neurons. Front. Cell. Neurosci. *15*, 759238. https://doi.org/10.3389/fncel.2021.759238.
41. Liu, C., Pitts, R.J., Bohbot, J.D., Jones, P.L., Wang, G., and Zwiebel, L.J. (2010). Distinct olfactory signaling mechanisms in the malaria vector mosquito Anopheles gambiae. PLoS Biol. *8*, e1000467. https://doi.org/10.1371/journal.pbio.1000467.
42. Lin, C.-C., and Potter, C.J. (2016). Editing transgenic DNA components by inducible gene replacement in Drosophila melanogaster. Genetics *203*, 1613–1628. https://doi.org/10.1534/genetics.116.191783.
43. Riabinina, O., Task, D., Marr, E., Lin, C.-C., Alford, R., O'Brochta, D.A., and Potter, C.J. (2016). Organization of olfactory centres in the malaria mosquito Anopheles gambiae. Nat. Commun. *7*, 13010–13012. https://doi.org/10.1038/ncomms13010.
44. Afify, A., Betz, J.F., Riabinina, O., Lahondère, C., and Potter, C.J. (2019). Commonly used insect repellents hide human odors from Anopheles mosquitoes. Curr. Biol. *29*, 3669–3680.e5. https://doi.org/10.1016/j.cub.2019.09.007.
45. Omondi, A.B., Ghaninia, M., Dawit, M., Svensson, T., and Ignell, R. (2019). Age-dependent regulation of host seeking in Anopheles coluzzii. Sci. Rep. *9*, 9699. https://doi.org/10.1038/s41598-019-46220-w.
46. Tallon, A.K., Hill, S.R., and Ignell, R. (2019). Sex and age modulate antennal chemosensory-related genes linked to the onset of host seeking in the yellow-fever mosquito, Aedes aegypti. Sci. Rep. *9*, 43. https://doi.org/10.1038/s41598-018-36550-6.
47. Pfister, P., Smith, B.C., Evans, B.J., Brann, J.H., Trimmer, C., Sheikh, M., Arroyave, R., Reddy, G., Jeong, H.-Y., Raps, D.A., et al. (2020). Odorant receptor inhibition is fundamental to odor encoding. Curr. Biol. *30*, 2574–2587.e6. https://doi.org/10.1016/j.cub.2020.04.086.
48. Donley, G., Sun, Y., Pass, G., Adler, P.H., Beard, C.E., Owens, J., and Kornev, K.G. (2022). Insect antennae: coupling blood pressure with cuticle deformation to control movement. Acta Biomater. *147*, 102–119. https://doi.org/10.1016/j.actbio.2022.05.044.
49. Konopka, J.K., Task, D., Poinapen, D., and Potter, C.J. (2022). Neurogenetic identification of mosquito sensory neurons. Preprint at bioRxiv. https://doi.org/10.1101/2022.11.22.517370.
50. Williams, C.G., Lee, H.J., Asatsuma, T., Vento-Tormo, R., and Haque, A. (2022). An introduction to spatial transcriptomics for biomedical research. Genome Med. *14*, 68. https://doi.org/10.1186/s13073-022-01075-1.
51. Konet, D.S., Anderson, J., Piper, J., Akkina, R., Suchman, E., and Carlson, J. (2007). Short-hairpin RNA expressed from polymerase III promoters mediates RNA interference in mosquito cells. Insect Mol. Biol. *16*, 199–206. https://doi.org/10.1111/j.1365-2583.2006.00714.x.
52. Hammond, A., Galizi, R., Kyrou, K., Simoni, A., Siniscalchi, C., Katsanos, D., Gribble, M., Baker, D., Marois, E., Russell, S., et al. (2016). A CRISPR-Cas9 gene drive system targeting female reproduction in the malaria mosquito vector Anopheles gambiae. Nat. Biotechnol. *34*, 78–83. https://doi.org/10.1038/nbt.3439.

## STAR★METHODS

### KEY RESOURCES TABLE

| REAGENT or RESOURCE | SOURCE | IDENTIFIER |
|---|---|---|
| Antibodies | | |
| Mouse anti-nc82 | DSHB | Cat# nc82; RRID: AB_2314866 |
| Rat anti-cd8 | Thermo Fisher Scientific | Cat# 14-0081-82; RRID: AB_467087 |
| Cy3 goat anti-mouse | Jackson ImmunoResearch | Cat# 115-165-166; RRID: AB_2338692 |
| Alexa 488 goat anti-rat | Invitrogen | Cat# A11034 |
| Chemicals, peptides, and recombinant proteins | | |
| 3-Methylpiperidine | Sigma-Aldrich | CAS# 626-56-2 |
| 3-Pyrroline | Sigma-Aldrich | CAS# 109-96-6 |
| Pyrrolidine | Sigma-Aldrich | CAS# 123-75-1 |
| 2-Acetylpyridine | Sigma-Aldrich | CAS# 1122-62-9 |
| Lactic acid | Sigma-Aldrich | CAS# 50-21-5 |
| l-octen-3-ol | Sigma-Aldrich | CAS# 3391-86-4 |
| Hexanoic acid | Sigma-Aldrich | CAS# 142-62-1 |
| N,N-Diethyl-m-toluamide (DEET) | Sigma-Aldrich | CAS# 134-62-3 |
| Lemongrass oil | Sigma-Aldrich | Product# W262404 |
| Butylamine | Sigma-Aldrich | CAS# 109-73-9 |
| Mineral oil | Sigma-Aldrich | CAS# 8042-47-5 |
| Critical commercial assays | | |
| In-Fusion HD Cloning | Clontech Labs | Clontech: 639,645 |
| Probe sets | Molecular Instruments, Inc | HCR v3.0 |
| IR7w *in situ* probe | Molecular Instruments, Inc | Probe Set ID: PRH968 |
| IR41C *in situ* probe | Molecular Instruments, Inc | Probe Set ID: PRH969 |
| IR41t.2 *in situ* probe | Molecular Instruments, Inc | Probe Set ID: PRH970 |
| IR75l *in situ* probe | Molecular Instruments, Inc | Probe Set ID: PRH971 |
| IR25a *in situ* probe | Molecular Instruments, Inc | Probe Set ID: PRK149 |
| IR8a *in situ* probe | Molecular Instruments, Inc | Probe Set ID: PRK150 |
| IR76b *in situ* probe | Molecular Instruments, Inc | Probe Set ID: PRI998 |
| IR41n *in situ* probe | Molecular Instruments, Inc | Probe Set ID: PRK696 |
| IR75h.2 *in situ* probe | Molecular Instruments, Inc | Probe Set ID: PRK697 |
| IR21a *in situ* probe | Molecular Instruments, Inc | Probe Set ID: PRK698 |
| IR75k *in situ* probe | Molecular Instruments, Inc | Probe Set ID: PRK699 |
| IR64a *in situ* probe | Molecular Instruments, Inc | Probe Set ID: PRK700 |
| IR41a *in situ* probe | Molecular Instruments, Inc | Probe Set ID: PRK974 |
| IR93a *in situ* probe | Molecular Instruments, Inc | Probe Set ID: PRK975 |

(*Continued on next page*)

*Continued*

| REAGENT or RESOURCE | SOURCE | IDENTIFIER |
|---|---|---|
| IR75d *in situ* probe | Molecular Instruments, Inc | Probe Set ID: PRK976 |
| IR31a *in situ* probe | Molecular Instruments, Inc | Probe Set ID: PRK977 |
| IR41t.1 *in situ* probe | Molecular Instruments, Inc | Probe Set ID: PRK978 |
| IR75g *in situ* probe | Molecular Instruments, Inc | Probe Set ID: PRL354 |
| IR7t *in situ* probe | Molecular Instruments, Inc | Probe Set ID: PRL355 |
| IR100a *in situ* probe | Molecular Instruments, Inc | Probe Set ID: PRL356 |
| Experimental models: Organisms/strains | | |
| *Anopheles coluzzii* N'Gousso | Insect Transformation Facility, Rockville, Maryland | N/A |
| *Anopheles coluzzii*: IR41c-T2A-QF2 | This paper | N/A |
| *Anopheles coluzzii*: QUAS-GCaMP6f/+ | Afify et al.[44] | N/A |
| *Anopheles coluzzii*: IR41c-T2A-QF2/+, QUAS-GCaMP6f/+ | This paper | N/A |
| *Anopheles coluzzii*: QUAS-CD8:GFP | Riabinina et al.[43] | N/A |
| *Anopheles coluzzii*: IR41c-T2A-QF2, QUAS-CD8:GFP | This paper | N/A |
| Oligonucleotides | | |
| IR41c_gRNA_Forward | This paper | GTTGCTCTCTGCTTGACAACATCCCCTTTA CCACGTTTTAGAGCTAGAAATAGCAAGTTA |
| IR41c_gRNA_reverse | This paper | TTCTAGCTCTAAAACCGTAGAAGTGTTCCA GAAATCAAGCAGAGAGCAACTCC |
| IR41c_5HA_Forward | This paper | GTGGTACGTAACGCGTTGGCAGCTCGGGA TTATAGGT |
| IR41c_5HA_Reverse | This paper | CGCGGCCCTCACGCGTGCACACGGTATAG TGTTGGCTGTAG |
| IR41c_3HA_Forward | This paper | AATTAGATCTCTCGAGCTGATCGCCATGAC GACATCT |
| IR41c_3HA_Reverse | This paper | ACGCAGCCGTCTCGAGCCGGCATAGCTGT TACCGATCATG |
| IR41c_ seq primer | This paper | TGTATTCCGTCGCATTTCTCTC |
| Recombinant DNA | | |
| pHACK-QF2-AgU6-mCherry | Deposited to Addgene | Cat#: 184530 |
| Software and algorithms | | |
| GraphPad software | www.graphpad.com | GraphPad Prism 8.0 & 9.0 |
| Fiji (ImageJ) | https://imagej.net/Fiji | N/A |
| Adobe Illustrator | Adobe, Inc. | Adobe illustrator CS6 |

## RESOURCE AVAILABILITY

### Lead contact

Resources and reagents are available from the lead contact Christopher J. Potter (cpotter@jhmi.edu) upon reasonable request.

### Materials availability

All unique/stable reagents generated in this study are available from the lead contact with a standard Materials Transfer Agreement.

### Data and code availability

- All data reported in this study will be shared by the lead contact upon request.

- This paper does not report original code.
- Any additional information required to reanalyze the data reported in this paper is available from the lead contact upon request.

## EXPERIMENTAL MODEL AND SUBJECT DETAILS

*Anopheles coluzzii* (N'Gousso strain; formerly *Anopheles gambiae* M form), were maintained under 12 h light/dark cycle at 28°C, and 72 ± 2% relative humidity. The larvae were fed ad libitum on TetraMin Tropical Flakes and Purina Cat pellets. The emerged adult mosquitoes were raised with 10% sucrose solution. To generate eggs, adult female mosquitoes were blood-fed on anesthetized mice or defibrinated sheep blood.

## METHOD DETAILS

### Hybridization chain reaction whole-mount fluorescence *in situ* hybridization (WM-FISH)

This assay was performed as previously described with some modifications.[34,38] All *in situ* probe reagents used were purchased from Molecular Instruments, Inc. Mosquito antennae aged 5-7 days post eclosion were dissected into CCD buffer (50 units of chitinase, 1000 units of chymotrypsin (25 mg of 40 units/mg), 10 mL HEPES larval buffer (119 mM NaCl, 48 mM KCl, 2 mM $CaCl_2$, 2 mM MgCl2, 25 mM HEPES), and 100 μL DMSO) on ice, then incubated for 25 min at 37°C on a rotator. Tissues were then pre-fixed in 4% paraformaldehyde (PFA) in PBT (1XPBS, 0.03% Triton X-100) for 24 h at 4°C. Tissues were washed with 0.1% PBS-Tween on ice, incubated for 1 h at RT in 80% methanol/20% DMSO. Tissues were incubated overnight at −20°C in absolute methanol. Using different series of graded Methanol/PBS-Tween (75% methanol, 50% methanol; 25% methanol; and 100% PBS-Tween in that order), tissues were rehydrated for 10 min on ice and washed with PBS-Tween at room temperature. This was followed by incubation in Proteinase K solution (20ug/mL) for 30 min and wash in PBS-Tween at room temperature. Tissues were post-fixed in 4% PFA in PBS-Tween at RT for 20 min. Tissues were washed in PBS Tween at room temperature three times for 15 min per wash, then pre-hybridized in pre-heated probe hybridization buffer at 37°C for 30 min. Tissues were incubated in probe solution (8 pmol in hybridization buffer) at 37°C for two nights. Thereafter, tissues were washed at least 5 times in pre-heated probe wash buffer at 37°C, then washed at room temp in saline sodium citrate dissolved in 1% Tween. Pre-amplification was performed using the amplification buffer at room temperature for 10 min, then incubated in the hairpin mixture (18 pmol snap-cooled hairpins in amplification buffer). Tissues were incubated overnight in the dark at room temperature. This was followed by a series of washes in saline sodium citrate solution performed at room temperature to remove excess hairpins. After, tissues were gently dipped in droplets of SlowFade Diamond (ThermoFisher S36972) at least three times to clear excess wash solution before mounting in SlowFade Diamond.

### Data acquisition

Following the *in situ* protocol, whole antenna tissues were mounted on slides and the IR-positive cells were counted manually under a Zeiss LSM 700 confocal microscope. Images were acquired at 512 x 512-pixel resolution with 0.58, 2.37 or 6.54 μm z-steps by using the Fluar 10x air M27, LCI 25x water immersion with Korr DIC M27. For illustration purposes, confocal images were exported as maximum intensity projection and processed in ImageJ and annotated on Adobe Illustrator. Images were linearly adjusted for brightness or contrast but were otherwise unmodified.

### Establishment of transgenic strains

To generate the *IR41c* knock-in, we used HACK method, previously utilized to create a pan-neuronal line of *Anopheles* mosquitoes.[49] The *IR41c* knock-in construct was generated using the *pHACK-QF2-AgU6* plasmid (Addgene# 80933) as the backbone. The *pHACK-QF2-AgU6* plasmid was generated based on the design of *Drosophila pHACK-QF2*.[42] The *Anopheles gambiae U6* promoters used to express two guide RNA cassettes were synthesized using gBlocks (Integrated DNA Technologies) based on the published *U6* promoter sequence,[51] and used to replace the *Drosophila U6:gRNA* cassettes in the *pHACK-QF2* vector. To clone the 3 main components (gRNAs, 5′ homology arm, and 3′ homology arm), the plasmid was digested with *BbsI* to clone in the gRNAs; *MluI* and *XhoI* to insert the 5′ homology arm and 3′ homology arm respectively and in that order. We amplified the two gRNAs using the *AgU6* template from the *pHACK-QF2-AgU6* plasmid while the homology arms were amplified from wild type *An. coluzzii* genomic DNA. The DNeasy Blood and Tissue Kit (Qiagen #69506) was used for genomic DNA extraction. The In-Fusion HD cloning system (Clontech, catalog number 639645) was used to construct the assembled plasmid.

Homology arms (HAs) from the targeted site extended at least 1kb (5HA = 1319 bp, 3HA = 1146 bp). The gRNAs were selected to target the first exon, approximately 174 bp apart. To minimize off targets, we searched for potential cleavage sites using an online tool (https://flycrispr.org/). Successful cloning into the vector was confirmed by Sanger sequencing (Genewiz) before injecting into the preblastodermal embryo. Below are the PCR primers used to clone the gRNAs, 5HA and 3HA into the *pHACK-QF2* plasmid organized from 5′ to 3′ direction. The In-Fusion 15bp overlap (italics), *IR41c* gene sequence (bold), and the aligning template (not bold) are shown below:

IR41c_*gRNA*_Forward = *GTTGCTCTCTGCTTG***ACAACATCCCCTTTACCAC**GTTTTAGAGCTAGAAATAGCAAGTTA.
IR41c_*gRNA*_Reverse = *TTCTAGCTCTAAAAC***CGTAGAAGTGTTCCAGAAAT**CAAGCAGAGAGCAACTCC.

IR41c_5HA_Forward = *GTGGTACGTAACGCGT***TGGCAGCTCGGGATTATAGGT**.
IR41c_5HA_Reverse = *CGCGGCCCTCACGCGT***GCACACGGTATAGTGTTGGCTGTAG**.
IR41c_3HA_Forward = *AATTAGATCTCTCGAG***CTGATCGCCATGACGACATCT**.
IR41c_3HA_Reverse = *ACGCAGCCGTCTCGAG***CCGGCATAGCTGTTACCGATCATG**.

The final plasmid construct *pHACK-AgIR41c* (250ng/ul) was co-injected into the embryos with plasmid p165 *AgVas2-hCas9* (250ng/ul)[52] as earlier described.[49] Injections were performed using FemtoJet 4x microinjector connected to TransferMan 4r micromanipulator (Eppendorf North America) under Nikon SZM-U microscope with 2xED Plan lens.

A total of 246 preblastoderm embryos were injected and 18 adult mosquitoes emerged from the injected population. The 18 $G_0$ mosquitoes were separated by sex and allowed to mate *en masse* in a cage of wild-type N'Gousso mosquitoes. $G_1$ progeny were scored at the larval stage for the mCherry fluorescent eye marker. From the $G_0$ crosses, 3 larvae produced mCherry + $G_1$ mosquitoes. In the second gonotrophic cycle, we identified 5 additional mCherry + $G_2$ mosquitoes. The *IR41c-T2A-QF2* lines were established from these 8 mCherry + mosquitoes. The *IR41c-T2A-QF2* line was screened for the presence of red eye marker and validated by Sanger sequencing of PCR products using these primers:

Forward *primer*: TGGCAGCTCGGGATTATA.
Reverse *primer*: GGCATAGCTGTTACCGATC.
Sequencing primer: TGTATTCCGTCGCATTTCTCTC.

The *IR41c-T2A-QF2* knock-in line was outcrossed to wild-type N'Gousso mosquitoes for 6 generations and maintained as heterozygous and homozygous stocks.

## Immunohistochemistry

As previously described,[43] the heads of adult *An. coluzzii IR41c-T2A-QF2*, *QUAS-CD8:GFP* transgenic mosquitoes aged 5-7 days post-eclosion were fixed for 3 h at 4°C in buffered 4% paraformaldehyde containing 0.1 M sodium phosphate buffer (Millonig's pH 7.4) and 0.25% Triton X-100. Thereafter, brains were dissected and permeabilized at 4°C overnight in PBS containing 4% Triton X-100 and 2% normal goat serum (NGS). Thereafter, brains were washed in PBT for 1 h at room temperature and counterstained with the primary monoclonal antibodies nc82 and CD8. Brains were incubated in mouse nc82 antibody (DSHB, 1:50) and rat anti-CD8 (Invitrogen 1:100) mix containing 2% NGS in PBT for 48 hrs at 4°C. This was followed by washing in PBT for 1 h at room temperature and incubated in secondary antibodies Cy3 goat anti-mouse (Jackson ImmunoResearch, 1:200) and Alexa 488 goat anti-rat (Invitrogen #A11034, 1:200) mix containing 2% NGS in PBT for 48 hrs at 4°C in the dark. Thereafter, secondary antibodies were washed off at least 3 times for 5min each in PBT and tissues were covered with a Vectashield coverslip and mounted for imaging under the microscope.

## Confocal microscopy

Antennae and brains were imaged on a Zeiss LSM 700 confocal microscope. Images were acquired at 512 x 512-pixel resolution with 0.58, 2.37 or 6.54 μm z-steps by using the Fluar 10x air M27, LCI 25x water immersion with Korr DIC M27, and C-Apochromat 63× water immersion objectives. For illustration purposes, confocal images were exported as maximum intensity projection and processed in ImageJ and annotated on Adobe Illustrator.

## Calcium imaging

We used a *IR41c-T2A-QF2*/+, *QUAS-GCaMP6f*/+ transgenic line to monitor odor-evoked calcium ion influx into IR41c-positive neurons. In this heterozygous line, it was possible to capture IR41c endogenous expression. *In vivo* calcium imaging protocol was performed as described.[44] Odorants were diluted in mineral oil (1:100), and a total of 20 μL of the odorant solution was pipetted onto a piece of filter paper (1 × 2 cm) that was positioned near the top of a Pasteur pipette. The Pasteur pipette was inserted into the larger hole of a plastic serological pipette (Denville Scientific Inc, 10 mL pipette). A stream of purified air (8.3 mL/s) was directed toward the antenna for odor delivery. A stimulus controller (Syntech) was used to deliver 1 s pulse of charcoal-filtered air (5 mL/s) into the Pasteur pipette for ~10 s after the beginning of each recording. To control for possible bias, odorants were randomized for each set of experiments, and new Pasteur pipettes were used for each recording. To capture the images, a EMCCD camera (Andor iXon Ultra, Oxford Instruments) was attached to the microscope. Andor Solis software was used to record videos which were processed on ImageJ/Fiji.

## Close proximity response assay

This assay was performed as described previously with slight modifications.[44] Sugar fed female wild-type and *IR41c* mutant mosquitoes, aged 5-8 days post eclosion, were tested singly in a cage (BugDorm, 30 × 30 × 30 cm). Mosquitoes were allowed to rest on the cage mesh walls for at least 5 min before they were approached with odorants. A total of 10 mosquitoes were tested in this assay for each odor. Odor was placed on a strip of filter paper inside a 1000 μL universal pipet tip of 5 cm length (VWR: Catalog #: 76,322-522). We ensured a distance of 0.5 cm between the pipette containing the odorant and the cage mesh. Upon approach with 1% odorant diluted in mineral oil, the time taken for the mosquito to fly away was recorded. A resting interval of 3 min was given to the mosquito before being approached with another odorant. Mineral oil was used as the solvent control.

## QUANTIFICATION AND STATISTICAL ANALYSIS

Data quantification and analysis were performed using the GraphPad Prism 9 software package (GraphPad Software, San Diego, CA). We performed two-sample T-tests and one-way ANOVA statistical tests in this study. Full statistical details can be found in the figure legends including statistical tests, number of samples and trials, and how statistical significance was determined.